Downloaded from orbit.dtu.dk on: Apr 20, 2024

DTU Library

# Numerical simulation of particles beneath a towed circular cylinder

Burgaard, Karen B.; Carstensen, Stefan; Fuhrman, David R.; O'Neill, Finbarr G.

*Published in:*
Coastal Engineering

*Link to article, DOI:*
10.1016/j.coastaleng.2024.104474

*Publication date:*
2024

*Document Version*
Publisher's PDF, also known as Version of record

Link back to DTU Orbit

*Citation (APA):*
Burgaard, K. B., Carstensen, S., Fuhrman, D. R., & O'Neill, F. G. (2024). Numerical simulation of particles beneath a towed circular cylinder. *Coastal Engineering*, *189*, Article 104474. https://doi.org/10.1016/j.coastaleng.2024.104474

**General rights**
Copyright and moral rights for the publications made accessible in the public portal are retained by the authors and/or other copyright owners and it is a condition of accessing publications that users recognise and abide by the legal requirements associated with these rights.

- Users may download and print one copy of any publication from the public portal for the purpose of private study or research.
- You may not further distribute the material or use it for any profit-making activity or commercial gain
- You may freely distribute the URL identifying the publication in the public portal

If you believe that this document breaches copyright please contact us providing details, and we will remove access to the work immediately and investigate your claim.

Coastal Engineering 189 (2024) 104474

Contents lists available at ScienceDirect

Coastal Engineering

journal homepage: www.elsevier.com/locate/coastaleng

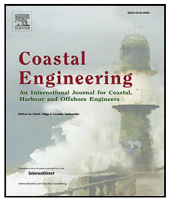

# Numerical simulation of particles beneath a towed circular cylinder

Karen B. Burgaard [a,*], Stefan Carstensen [b], David R. Fuhrman [b], Finbarr G. O'Neill [a]

[a] Technical University of Denmark, National Institute of Aquatic Resources, Section for Fisheries Technology, 9850 Hirtshals, Denmark
[b] Technical University of Denmark, Department of Civil and Mechanical Engineering, Section for Fluid Mechanics, Coastal and Maritime Engineering, 2800 Kgs. Lyngby, Denmark

ARTICLE INFO

*Keywords:*
Particle path model
Suspended particles
Towed fishing gear
Bottom trawl
Sea stars
Towed cylinder

ABSTRACT

This study investigates particle dynamics around a towed circular cylinder near a wall. The flow field obtained from a numerical model based on the Reynolds-Average Navier–Stokes equations is utilized to estimate the particle trajectories computed using a Lagrangian approach. The simulated flow resembles a towed fishing gear and the particles which represent sea stars, muscles, and sediments are seeded at the seabed. The ejection of particles from the seabed is related to the upward flow induced by lee-wake vortex shedding. The effect of the gap between the cylinder and the seabed is investigated, where an increased distance leads to fewer ejected particles and distinct trajectories. Furthermore, for the same relative distance to the seabed, a larger diameter cylinder, and hence a different relative initial position and Reynolds number, leads to fewer ejected particles. The optimal position of the fishing net of a towed fishing gear relative to the cylinder is investigated based on the trajectories.

## 1. Introduction

The hydrodynamics around a circular cylinder near a wall has been investigated in great detail both experimentally and numerically (e.g. Sumer and Fredsoe (2006), Bearman and Zdravkovich (1978), Hourigan et al. (2013), Ong et al. (2010)) due to the many engineering applications such as marine pipelines. Flow characteristics such as the velocity field and vortex shedding have been seen to be dependent on the gap between the wall and the cylinder $e$ henceforth referred to as clearance. The dynamics of particles close to the cylinder and in the wake are important for many applications such as scour predictions (Zhao and Cheng, 2008) or for the selective and environmental performance of towed fishing gears.

Demersal towed fishing gears are multi-species fishing gears that exploit species that live close to or on the seabed and are responsible for approximately 25% of global landings of wild capture fish (Perez Roda et al. 2019). There are many designs and sizes, and one of the most commonly used types is the beam trawl, which consists of a circular cylinder/beam that is used to keep the net open, and which is towed across the seabed behind a fishing vessel. There are, however, concerns about the environmental impact on the seabed and the capture of unwanted bycatch species. Many gears have been developed and modified to improve the selectivity and decrease the impact on the seabed (e.g. Bromhall et al. (2022), Kennelly and Broadhurst (2021)), nevertheless, the fishing industry still faces the challenge of improving the selectivity of the fishing gear and reducing the impact on the seabed.

The hydrodynamics around the beam in the fishing gear potentially affect the catch efficiency of the fishing gear, since some demersal species may be influenced by the flow. The sea star fishery is an example of a fishery where the hydrodynamics are expected to play an important role. Sea stars have a density close to water (Burgaard et al., 2023b), hence they are expected to be easily affected by their surrounding hydrodynamics. Furthermore, towed fishing gear leads to the suspension of particles (O'Neill and Summerbell, 2016), and sea stars are expected (at least to a first approximation) to respond like particles since they lie on the seabed and have very little swimming capacity.

Sea stars are major predators of molluscs and benthic invertebrates and can cause considerable impact on both natural populations of shellfish and cultivated beds. The common sea star (*Asterias rubens*) ranges from Senegal to Norway in northwestern Europe (Budd, 2022) and poses a large threat to the fishery of species such as blue mussels (*Mytilus edulis*) and scallops (*Pecten maximus*) (Dare, 1982; Calderwood et al., 2015; Magneson and Redmond, 2012). Several methods for protecting mussels from sea stars have been attempted, including trawling, hand-picking, and mopping (Barkhouse et al., 2007). Trawling for sea stars originated as a method to protect the shellfish, but harvested sea stars are now exploited as a source of protein. The sea stars are

* Corresponding author.
*E-mail address:* kbur@aqua.dtu.dk (K.B. Burgaard).

https://doi.org/10.1016/j.coastaleng.2024.104474
Received 27 April 2023; Received in revised form 28 August 2023; Accepted 23 January 2024
Available online 24 January 2024
0378-3839/© 2024 The Authors. Published by Elsevier B.V. This is an open access article under the CC BY license (http://creativecommons.org/licenses/by/4.0/).

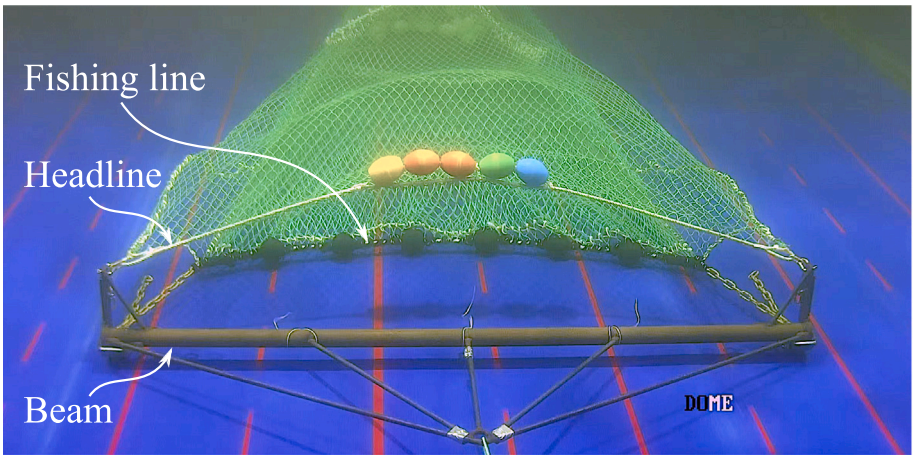


**Fig. 1.** Fishing gear used in the sea star fishery.

processed into protein powder and used as a supplement for animal feed. For processing the catch of sea stars has to be clean without significant mussel bycatch.

Fig. 1 shows a beam trawl commonly utilized in the sea star fishery. The beam trawl consists of a beam at a fixed position above the seabed. A fishing net is supported by the beam where a fishing line and a headline constitute the mouth of the fishing net and are attached to the beam. The fishing line is positioned at the ground and keeps the fishing net near the seabed while the headline is at the top of the net. Buoys are attached to the headline to keep the net open vertically. The position of the fishing line and the headline have to be positioned correctly relative to the beam for the catch efficiency of the fishing gear to be optimal. To position the fishing line and the headline in the most optimal position, the hydrodynamical effect, and hence the particle trajectories have to be known.

The trajectories of suspended particles have been investigated previously around a circular cylinder (e.g. Yao et al. (2009)) and a cylinder near a wall (Ong et al., 2012). The studies showed that the settling velocity of the particles and vortex shedding are very important for the trajectories and that the paths are a complex interaction between particle weight and distance to the wall.

The present study investigates numerically how the hydrodynamics around a towed cylinder near a wall affects particles close to the wall. The velocity field is determined and the dynamics of particles with initial position close to the wall are investigated using a Lagrangian approach. The weight of the particles is taken into account by including the settling velocity of the particles. The effect of the clearance on the particle trajectories is examined as well as the significance of the Reynolds number. The trajectories are utilized to estimate the optimal position of the fishing line and the headline of the fishing gear used in the sea star fishery to increase the catch efficiency.

## 2. Materials and methods

### 2.1. Flow-field simulation

The numerical simulations were based on two-dimensional unsteady incompressible Reynolds-Averaged Navier–Stokes (RANS) equations, with the $k$-$\omega$ turbulence model of Wilcox (2006) utilized for closure, as implemented (and made available) by Li et al. (2022). The numerical simulations were performed in OpenFOAM to obtain the velocity field and post-processing was performed in Matlab to obtain particle trajectories. The simulations are a two-dimensional version of the simulation in Burgaard et al. (2023a) which was validated from experimental data. The simulations were run on a high performance computing cluster where the CPU time was approximately 1 h on 16 processors for the OpenFOAM simulations.

A circular cylinder near a moving wall is simulated in a cross-flow as presented in the definition sketch in Fig. 2. Two cylinder diameters, $d = 0.08$ m and 0.16 m, will be used in the investigation. A coordinate system with $x$ in the horizontal and $z$ in the vertical direction is adopted. The origin of the coordinate system is in the center of the cylinder. An additional vertical axis $\xi$ is also introduced with origin at the wall. The clearance is varied between $0.5 \leq e/d \leq 1$. The parameters in the simulation have been chosen according to the sea star fishery practice.

The boundaries of the numerical domain are far from the cylinder to eliminate far-field effects and span at least $10d$ on the vertical axis, $10d$ upstream, and $25d$ downstream of the cylinder. A structured grid was utilized in the simulations with a resolution of 120 cells in the circumference of the cylinder and decreasing resolution away from the cylinder except at the seabed. A close-up of the utilized mesh is shown in Fig. 3. A uniform mean velocity profile is implemented at the left inlet with $U_0 = 1$ m/s and the lower wall has velocity $U_0$ as well hence no boundary layer forms at this wall since the bottom moves at the same velocity as the upstream flow, the same conditions as if the fluid and seabed were still and the cylinder was towed with $U_0$ are obtained as would be the case for a towed fishing gear. A slip boundary condition is utilized for the upper boundary, a zero gradient at the right, and a no-slip at the surface of the cylinder ($u = w = 0$), and the turbulent kinetic energy was set to $\partial k/\partial n = 0$ (Fuhrman et al., 2010).

### 2.2. Particle trajectories

A Lagrangian approach is utilized to estimate the location of the particles in the flow around the cylinder. The particles are assumed to have a settling velocity $w_s$ and no volume. Interactions between the particles and the flow are not taken into account, hence a one-way coupling is utilized in this study. The settling velocity of the particles is based on the settling velocity of sea stars as determined in Burgaard et al. (2023b). Here, the settling velocity was determined to be a function of the arm length of the sea star in the range $0.08 \leq w_s \leq 0.22$ m/s but for simplicity and since the size of the particles is not considered, a value of $w_s = 0.1$ m/s is used, hence $w_s/U_0 = 0.1$. Interaction between the particles is not considered in the present study.

Based on these assumptions, a simplified method can be used to determine the trajectory of the particles

$$x_p^{(n+1)} = x_p^{(n)} + u_p^{(n)} \Delta t \tag{2.1}$$

$$z_p^{(n+1)} = z_p^{(n)} + (w_p^{(n)} - w_s)\Delta t \tag{2.2}$$

where $x_p$ is the $x$-coordinate of the particle, and $z_p$ the $z$-coordinate. The superscript indicates the discrete time level and $\Delta t$ is the time

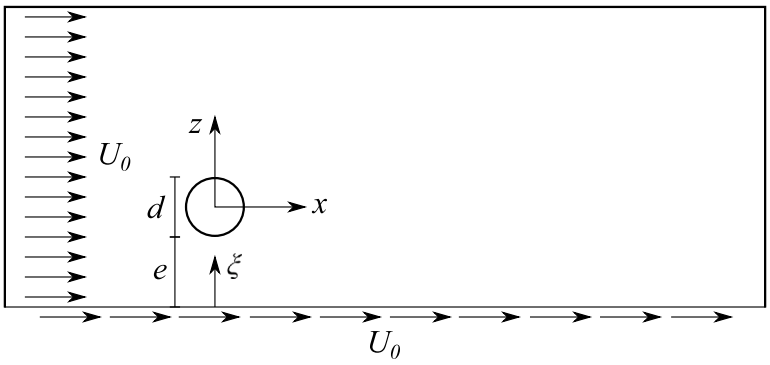


**Fig. 2.** Definition sketch for flow around circular cylinder close to a plane wall. Wall and uniform flow has the velocity $U_0$.

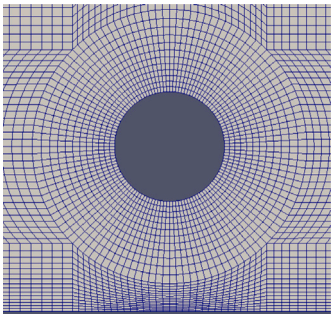

**Fig. 3.** Close-up of mesh around the cylinder.

step. The velocities $u_p$, and $w_p$ are the velocities of the particle in the two directions. The velocities are determined from the velocity field obtained from the CFD model as described in Section 2.1 and they are dependent on the position of the particle in the flow. The particle velocities are extracted from the flow field at each time step.

The particles in the model are intended to loosely represent sea stars lying on the seabed. Therefore, the initial vertical position of the particles $\xi_0$ is estimated from half the thickness of the sea stars determined by Burgaard et al. (2023b). The initial horizontal positions are determined from the characteristic length of a vortex shedding cycle ($U_0/f_v = d/St$) where 50 particles equidistantly cover a cycle. Here $f_v$ is the vortex shedding frequency and $St = f_v d/U_0$ is the Strouhal number. A lower vertical limit given by $\xi_0$ is implemented such that the particles cannot move below the seabed. The particles will have the horizontal velocity $u_p = U_0$ such that the particles remain at the seabed unless ejected into the water column.

## 3. Results and discussion

### 3.1. Particle paths

The trajectories of the particles and their movement is related to the formation and shedding of vortices on the downstream side of the cylinder. Fig. 4 shows the formation of vortices on either side of the cylinder and a corresponding schematic diagram of the flow directions. Vortices are shed in an alternating manner from the upper and lower side of the cylinder. A vortex formed at the lower side of the cylinder will cause an upward flow near the bed, point A in Fig. 4(a), which will be supported by an upward flow from the vortex shed from the upper side beforehand. The upward flow will potentially cause ejection of particles. A vortex formed at the upper side of the cylinder will cause a downward flow, point B in Fig. 4(b), which will not cause ejection of particles. The particles are transported by the vortex they are ejected by and will effectively move in curved paths aligning with the induced velocities of the vortex. The paths will be investigated in the following based on the velocity components in the vortices.

The position of the particles is visualized over two vortex shedding cycles in Fig. 5 for the small cylinder with $e/d = 0.5$. The velocity field has been divided into the mean horizontal (left) and mean vertical (right) velocity component in the figure where the mean horizontal and vertical velocity components can be explained from the vortices, based on the schematic diagrams in Fig. 4. From Fig. 5b and d, it is seen that the particles are ejected from the seabed when the particles are in a zone with positive mean vertical velocity (E1) while they stay at the lower limit in a zone with negative mean vertical velocity (E2). The upward flow in E1 corresponds to point A in Fig. 4(a) while E2 corresponds to point B in Fig. 4(b).

The ejected particles continue to rise (Fig. 5f and h) as long as they are in a zone with positive mean vertical velocities if the mean


(a) Vortex shedding from lower side of cylinder. Ejection of particles at point A.

(b) Vortex shedding from upper side of cylinder. No ejection of particles at point B.

**Fig. 4.** Sketch of vortex shedding from the cylinder including schematic diagram of flow directions.

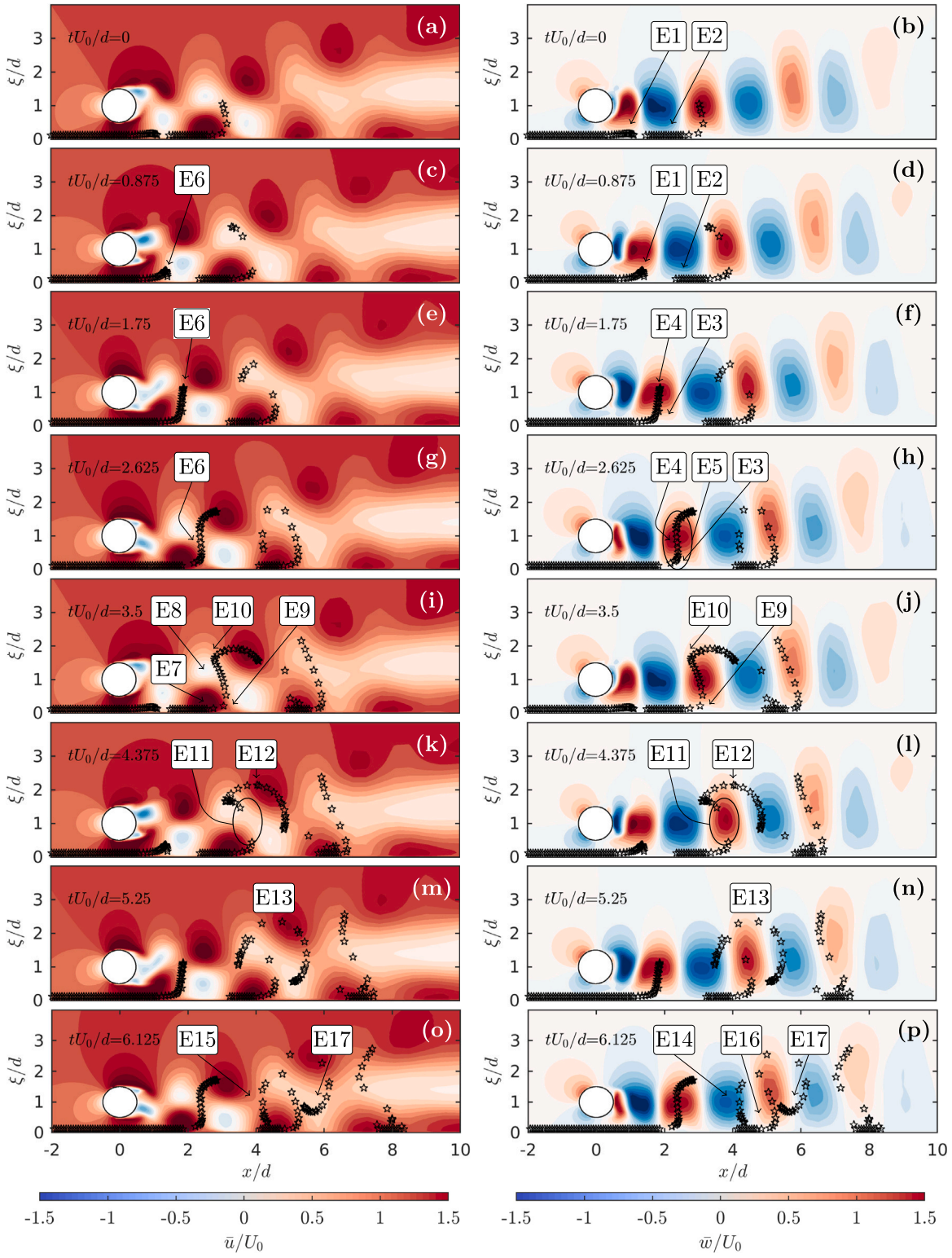


**Fig. 5.** Particle paths over two vortex shedding cycles. $d = 0.08\,\mathrm{m}$ and $e/d = 0.5$. Left: mean horizontal velocity component. Right: mean vertical velocity component. E1: Ejection. E2: No ejection. E3: Small mean vertical velocity. E4: High mean vertical velocity. E5: Vertical line of particles. E6: Mean horizontal velocity close to $U_0$. E7: High mean horizontal velocity. E8: Low mean horizontal velocity. E9: Particles further downstream. E10: Particles further upstream. E11: Gap between particles. E12: Half-circle of particles. E13: Particles from half-circles spread out to zones with positive and negative mean vertical velocity. E14: Particles settling. E15: Large mean horizontal velocity. E16: Ejection. E17: Particles raise for the second time.

velocities are larger than the settling velocity. The vertical motion is lowest at the edges of the zone (E3) and fastest in the middle of the zone (E4). This leads to a temporary vertical line of particles as seen in Fig. 5h (E5) where an accumulation of particles occurs above and below the center of the zone with positive mean vertical velocities. Compared to Fig. 4(a), this is between the two vortices where an upward motion is occurring.

While the particles are moving upward in the vertical direction, they are also moving further downstream. The particles have a positive mean horizontal velocity (Fig. 5c, e, and f) which is close to $U_0$ (E6). The lowest positioned particles in the vertical line (Fig. 5g) will be in a zone with higher mean horizontal velocities close to the seabed (E7) due to the velocities in the vortex formed at the lower side. The highest positioned particles will, on the other hand, be in a zone with zero or slightly negative mean horizontal velocities (E8) corresponding to the upper part of the same vortex which causes a flow in the opposite direction of the incoming flow.

The particles that initially formed a vertical line (Fig. 5g and h, E5), now become horizontally separated (Fig. 5i and j), where the lower particles have moved further downstream (E9) than the upper ones (E10). This effect has increased even further in Fig. 5k and l where a large gap (E11) is seen between the two groups of particles. In the upper group, some of the particles have a large mean horizontal velocity and also have a positive mean vertical velocity while some have a close to zero mean horizontal and vertical velocity. The horizontal velocity of the particles depends on which vortex the particles are transported by. The upward flow ejecting the particles is present between two vortices as seen in Fig. 4(a), where the particles will be transported either up- or downstream depending on the vortex they are transported by. This will cause the particles to spread out, which forms a half circle (Fig. 5k and l, E12). The particles are spread out even further and will be in several velocity zones (Fig. 5m and n, E13). Some of the particles will now have obtained a negative mean vertical velocity causing them to flow downward (Fig. 5p, E14) whereafter their mean horizontal velocity is increased (E15). Some are still being ejected from the seabed (Fig. 5o, E16) while others have obtained a downward motion whereafter they will be transported horizontally. They will then be lifted by the upward moving fluid (E17), and their cycle continued. The vortices will fade and the energy dissipate as they move downstream while they also deform due to the proximity of the wall. The settling velocity of the particles and the reduced velocities in the vortices eventually cause the particles to fall out of the vortices. In Fig. 5i and j, the shedding of the next vortex has begun ejecting particles from the seabed and the process is repeated.

The trajectories of the particles are dependent on the vortices. Therefore, the particles are initially positioned equidistantly and cover a distance comparable to the characteristic length of the vortex shedding cycle. This allows the determination of the probability of a particle being at a location in the wake of the cylinder. To this end the wake is divided into bins. The proportion of particles passing through each bin during a cycle is determined where each particle can only be counted once in each bin. By determining the proportion of particles in each bin the probability of finding a particle downstream of the cylinder can be visualized and hence the optimal position of the fishing net is determined. Fig. 6a shows the result of performing this analysis on the particle trajectories visualized in Fig. 5.

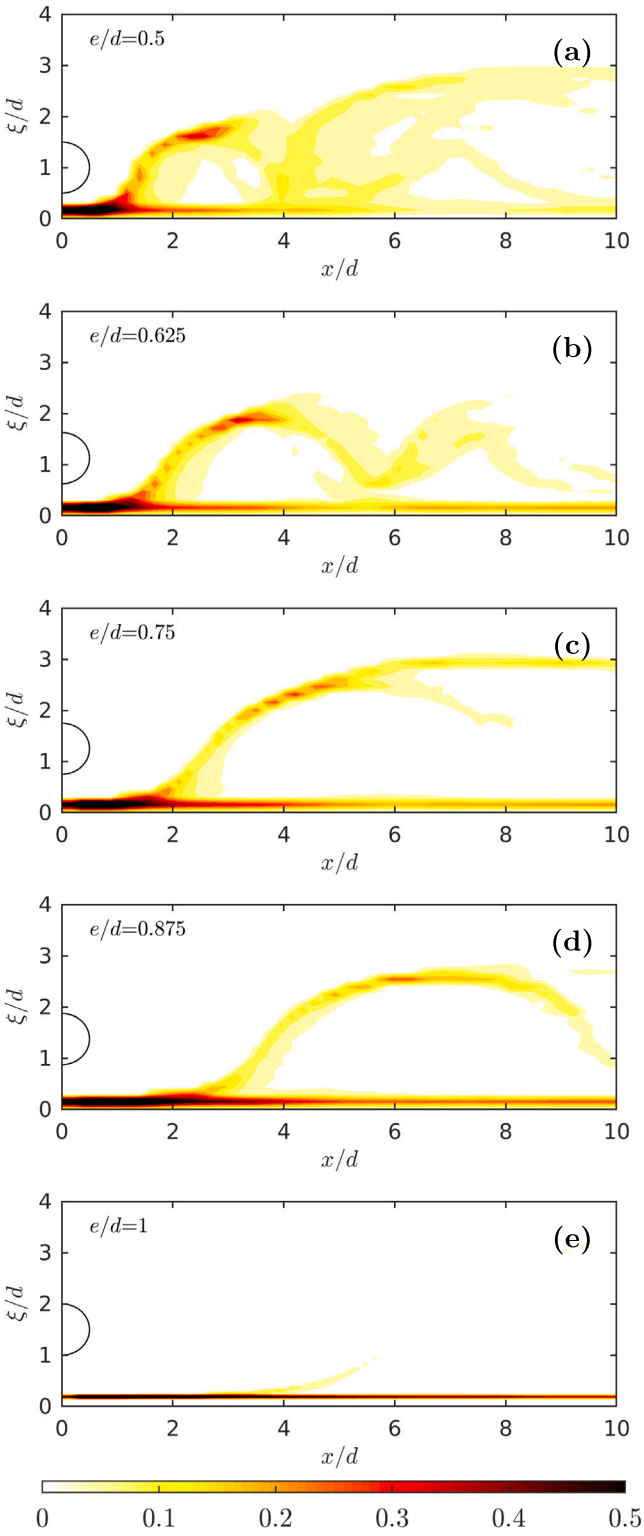


**Fig. 6.** Proportion of particles in a location based on the particle paths downstream of the cylinder. The clearance is varied between $e/d = 0.5$–1.

### 3.2. Effect of gap ratio

Five gap ratios in the interval $0.5 \leq e/d \leq 1$ are selected to study the effect of the gap ratio on the particle paths. The particles were seen to be dependent on the vortex shedding cycle, and especially on the positive mean vertical velocity ejecting the particles from the seabed and into the water column. The vortex shedding and wake are dependent on the gap ratio and hence are expected to affect the predicted trajectories. Fig. 6 presents the proportion of particles in a location downstream of the cylinder. The proportions of particles are determined from 10 vortex shedding cycles and a $x$-$\xi$-coordinate system is utilized to ease comparison between the gap ratios.

The particles are not ejected from the seabed before being downstream of the cylinder since the positive mean vertical velocities from the shedding on the lower side of the cylinder are required. A large

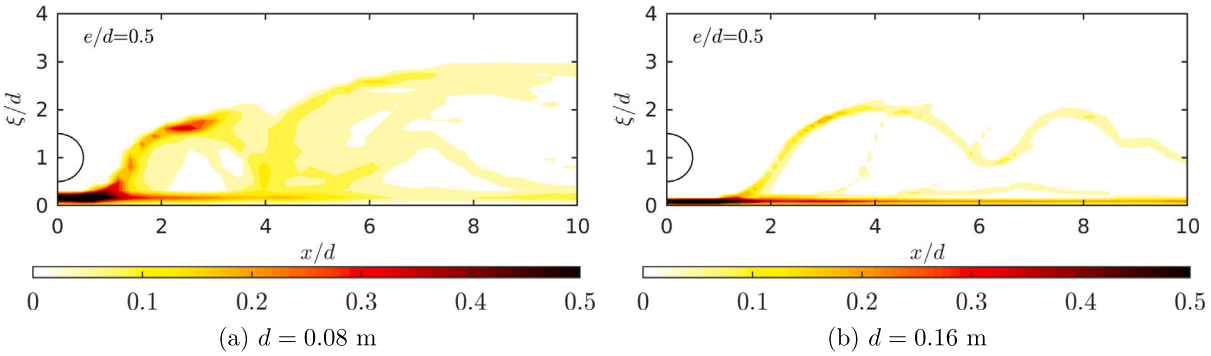


(a) $d = 0.08$ m (b) $d = 0.16$ m

**Fig. 7.** Proportion of particles in a location based on the particle paths downstream of cylinders with different diameters.

proportion of the particles are ejected for $e/d = 0.5$ with only a few remaining at the seabed. The ejection occurs gradually but with a majority of the ejections around $x/d = 1$. The sea stars must be ejected before they can be caught in the net. Sea trials in the sea star fishery were conducted by Burgaard et al. (2023c), where an increase in clearance caused fewer sea stars to be caught. This is similar to the findings in the present study where fewer sea stars are ejected with a larger clearance.

The ejection of particles is seen from Fig. 6 to occur at a distance of $x/d = 1$ from the origin for $e/d = 0.5$ and increases to $x/d = 4$ for $e/d = 1$. Not only does the distance from the cylinder increase but the number of particles ejected reduces gradually as the clearance increases. Only a small proportion are ejected for $e/d = 1$ leading to only a faint contour away from the seabed while the contour at the seabed is very distinct. The reduced number of particles ejected with increasing clearance is due to the velocity field. The positive mean vertical velocities from Fig. 5 were shown to occur in circular zones. Decreasing the clearance causes the vortex shedding to occur closer to the seabed. The area where the positive mean vertical velocities are large enough to overcome the settling velocity will increase leading to increased particle ejection. Furthermore, the mean velocities are larger causing the path of the particles to be different.

The trajectories in Fig. 6 are noticeably different depending on the clearance. The contour for $e/d = 0.5$ is based on many distinctive paths and the particles are most likely moving up and down with the vortex shedding. This leads to a half-circle shape closest to the cylinder. Some of the paths approach $\xi/d = 3$ for $x/d = 10$ while other particles are close to settling. A similar tendency is seen for $e/d = 0.625$ but here the paths approaching $\xi/d = 3$ are not present and the first half-circle has a larger diameter. The diameter of the half-circle is increased even further for $e/d = 0.75$ and the upper contour line approaching $\xi/d = 3$ is present again. For $e/d = 0.875$, the half-circle has become flatter, suggesting that the particles follow the upper boundary of the wake before they start to settle around $x/d = 8$. Not enough particles are ejected for $e/d = 1$ to indicate the trajectories. For $0.5 \leq e/d \leq 0.875$, it is common that the majority of the particles have not settled within $x/d = 10$.

### 3.3. Effect of diameter

Fig. 7 shows the proportion of particles in a location downstream of cylinders with $e/d = 0.5$ and $d = 0.08$ m and 0.16 m, respectively. Fig. 7(a) is similar to the one in Fig. 6 but is shown here together with Fig. 7(b) to ease comparison. From Sumer and Fredsoe (2006) it is known that the induced mean velocities at the seabed are similar in the two cases, however, the two contours are distinct. The differences in the trajectories are effectively caused by the difference in the ratio of the initial position and the diameter $\xi_0/d$. Recall that the thickness of the sea stars was used to estimate $\xi_0$ and hence have to remain the given value while the diameter can be altered. The Reynolds number given by $Re = U_0 d/\nu$ is also different where $\nu = 10^{-6}$ m$^2$/s is the kinematic viscosity. A large diameter cylinder causes the majority of the ejected particles to be lifted at $x/d \approx 1.5$ which is slightly higher than for the small cylinder. More noticeable, the number of particles being ejected for the large cylinder is significantly smaller than for the small cylinder. This is similar to the findings in the sea star fishery (Burgaard et al., 2023c) where a larger beam caused fewer sea stars to be caught for the same relative clearance. The shapes of the paths are similar for the two cylinders but the half circle of the large cylinder has a larger relative diameter, hence the shape of the contour is somewhat similar to that obtained for $e/d = 0.625$ in Fig. 6.

### 3.4. Position of fishing net

The position of the fishing net in the sea star trawl can be chosen based on the estimates of the particle locations. In the fishery, the aim is to increase the efficiency of the fishing gear, hence catching as many sea stars as possible. From Fig. 6, it was shown that for the majority of the ejected particles, the ejection occurred before $x/d = 4$ for all the investigated clearances. The position of the fishing line has to be at a $x$-position after particle ejection for the particles to enter the fishing net. The particles do not settle within $x/d = 10$ so there is no upper limit to the position of the fishing line within the investigated interval. However, some of the particles are close to settling and a net position of $x/d < 10$ is recommended. The position of the headline has to be selected such that the particles are not raised above the headline and escape before entering the net. The maximal position the particles reach is $\xi/d = 3$ for all clearances, hence the particles will not escape if the headline is at $\xi/d > 3$ for all $x$-positions. A lower position of the headline can be selected if the horizontal position is close to the cylinder where the particles are still being ejected. The same recommendations are given for the large cylinder given the contours in Fig. 7. The fishing net will most likely have a limited effect on the trajectories of the sea stars if the headline is above the particle paths and the fishing line is positioned more than $x/d = 4$ downstream of the beam, where ejection has occurred. The net will be surrounding, but not interfering with, the trajectories.

The sea stars were, as a first approximation, modeled as particles without taking their volume or interaction with the flow into account, hence the particles were affected by the mean flow and the settling velocity. The Stokes number $Stk$, which describes the particle response time compared to the characteristic flow time, is in reality $Stk \gg 1$. According to the study by Benavides and van Wachem (2008) a $Stk \gg 1$ indicates that the effect of the eddies on the path of the particle is reduced. However, due to the similar tendencies obtained in the actual practice of the sea star fishery (Burgaard et al., 2023c), the simplified model can be used to give a first estimate of the particle paths.

The settling velocity in the model was estimated from the settling velocity of sea stars. Not only sea stars but also mussels and cockles among others are affected by the hydrodynamics and possibly be

ejected when the fishing gear is towed. A similar analysis could be conducted utilizing the settling velocity of shellfish. The settling velocity has a large influence on the particle paths (e.g. Fredsoe and Deigaard (1992), Ong et al. (2012)), and hence the ejection and trajectories are expected to be different. If the location of both the shellfish and sea stars is known, the position of especially the fishing line can be strategically positioned to avoid the shellfish while catching the sea stars and thereby increase the selectivity of the fishing gear. Furthermore, the model can be utilized to optimize the clearance and size of the cylinder to obtain the optimal hydrodynamical conditions.

Finally, it should be noted that comparison with data is required to validate the model and a firm conclusion on the results given. The results appear to be physically proper and show similar tendencies as in Burgaard et al. (2023c). The results give insight into some of the features regarding the ejection of particles from the seabed around a circular cylinder near a moving wall.

## 4. Conclusions

The velocity field around a circular cylinder near a moving wall, resembling a towed fishing gear, has been determined from a RANS model and utilized to investigate particle dynamics. The initial position of the particles was close to the wall. The particles were seen to be ejected from the seabed when positive mean vertical velocity occurred near the seabed due to vortex shedding. The particle paths were seen to be affected by the mean horizontal and vertical velocities in the vortex shedding.

The trajectories are affected by the clearance, the distance between the seabed and the cylinder, where an increased clearance leads to significantly fewer particles ejected from the seabed. Almost none of the particles are ejected for $e/d = 1$ while a large proportion is ejected for $e/d = 0.5$. Furthermore, the particles were raised from the seabed close to the cylinder for a small clearance and the shape of the trajectories changes. The paths form a half-circle closest to the cylinder where the diameter of the half-circle increase with increasing clearance. The effect of the diameter of the cylinder was investigated utilizing cylinders with two different diameters and the same relative clearance $e/d = 0.5$ but different relative initial positions $\xi_0/d$. Fewer particles were ejected for the large diameter where the dominating trajectory was similar to the shape obtained for $e/d = 0.625$ utilizing the small cylinder.

Based on the particle trajectories, the optimal position of the fishing line in the towed fishing gear is determined to be $x/d > 4$ for the fishing gear to be the most efficient. The particles have not settled within $x/d = 10$ but are close to settling, hence it is recommended to position the fishing line closer to the cylinder than $x/d = 10$. The headline should be positioned at $\xi/d > 3$ for the particles to not escape above the headline.

## CRediT authorship contribution statement

**Karen B. Burgaard:** Conceptualization, Formal analysis, Investigation, Visualization, Data curation, Methodology, Writing – original draft, Writing – review & editing. **Stefan Carstensen:** Supervision, Methodology, Funding acquisition, Writing – review & editing. **David R. Fuhrman:** Supervision, Methodology, Funding acquisition, Writing – review & editing. **Finbarr G. O'Neill:** Supervision, Funding acquisition, Methodology, Project administration, Writing – review & editing.

## Declaration of competing interest

The authors declare that they have no known competing financial interests or personal relationships that could have appeared to influence the work reported in this paper.

## Data availability

No data was used for the research described in the article.

## Acknowledgments

The research leading to these results has received funding from the European Fisheries Fund and is part of the project "Using hydrodynamics to develop more selective fishing gears" (HydroSel), Grant number 33113-I-19-130.

## References

Barkhouse, C., Niles, M., Davidson, L.A., 2007. A literature review of sea star control methods for bottom and off bottom shellfish cultures. In: Canadian Industry Report of Fisheries and Aquatic Sciences 279. p. vii + 38.

Bearman, P.W., Zdravkovich, M.M., 1978. Flow around a circular cylinder near a plane boundary. J. Fluid Mech. 89 (1), 33–47.

Benavides, A., van Wachem, B., 2008. Numerical simulation and validation of dilute turbulent gas-particle flow with inelastic collisions and turbulence modulation. Powder Technol. 182 (2), 294–306.

Bromhall, K., Dinesen, G.E., McLaverty, C., Eigaard, O.R., Petersen, J.K., Saurel, C., 2022. Experimental effects of a lightweight mussel dredge on benthic fauna in a eutrophic MPA. J. Shellfish Res. 40 (3), 519–531.

Budd, G.C., 2022. Asterias rubens common starfish. Tyler-Walters H. and Hiscock K. Marine Life Information Network: Biology and Sensitivity Key Information Reviews (online), URL https://www.marlin.ac.uk/species/detail/1194.

Burgaard, K.B., Carstensen, S., Fuhrman, D.R., Larsen, B.E., O'Neill, F.G., 2023a. Experimental and numerical investigation of a disc-attached cylinder near a wall. Ocean Eng. 285 (2), 115366.

Burgaard, K.B., Carstensen, S., Fuhrman, D.R., Saurel, C., O'Neill, F.G., 2023b. Morphology and settling velocity of sea stars (Asterias rubens). J. Mar. Sci. Eng. 11 (2), 296.

Burgaard, K.B., Carstensen, S., Fuhrman, D.R., Saurel, C., O'Neill, F.G., 2023c. Using hydrodynamics to modify fishing performance of a demersal fishing gear. Fish. Res. 268, 106831.

Calderwood, J., O'Connor, N.E., Roberts, D., 2015. Efficiency of starfish mopping in reducing predation on cultivated benthic mussels (Mytilus edulis Linnaeus). Aquaculture 452, 88–96.

Dare, P.J., 1982. Notes on the swarming behaviour and population density of Asterias rubens L. (Echinodermata: Asteroidea) feeding on the mussel, Mytilus edulis L.. J. du Conseil / Conseil Permanent International pour l'Exploration de la Mer 40, 112–118.

Fredsoe, J., Deigaard, R., 1992. Mechanics of Coastal Sediment Transport. World Scientific.

Fuhrman, D.R., Dixen, M., Jacobsen, N.G., 2010. Physically-consistent wall boundary conditions for the k-$\omega$ turbulence model. J. Hydraul. Res. 48, 793–800.

Hourigan, K., Rao, A., Brøns, M., Leweke, T., Thompson, M.C., 2013. Vorticity generation and wake transition for a translating circular cylinder: Wall proximity and rotation effects. J. Wind Eng. Ind. Aerodyn. 122, 2–9.

Kennelly, S.J., Broadhurst, M.K., 2021. A review of bycatch reduction in demersal fish trawls. Rev. Fish Biol. Fish. 31 (2), 289–318.

Li, Y., Larsen, B.E., Fuhrman, D.R., 2022. Reynolds stress turbulence modelling of surf zone breaking waves. J. Fluid Mech. 937, A7.

Magneson, T., Redmond, K.J., 2012. Potential predation rates by the sea stars Asterias rubens and Marthasterias glacialis, on juvenile scallops, Pecten maximus, ready for sea ranching. Aquacult. Int. 20, 189–199.

O'Neill, F.G., Summerbell, K.D., 2016. The hydrodynamic drag and the mobilisation of sediment into the water column of towed fishing gear components. J. Mar. Syst. 164, 76–84.

Ong, M.C., Holmedal, L.E., Myrhaug, D., 2012. Numerical simulation of suspended particles around a circular cylinder close to a plane wall in the upper-transition flow regime. Coast. Eng. 61, 1–7.

Ong, M.C., Utnes, T., Holmedal, L.E., Myrhaug, D., Pettersen, B., 2010. Numerical simulation of flow around a circular cylinder close to a flat seabed at high Reynolds numbers using a $k$–$\epsilon$ model. Coast. Eng. 57, 931–947.

Sumer, B.M., Fredsoe, J., 2006. Hydrodynamics Around Cylindrical Structures. World Scientific.

Wilcox, D.C., 2006. Turbulence Modeling for CFD, third ed. DCW Industries.

Yao, J., Zhao, Y., Hu, G., Fan, J., Cen, K., 2009. Numerical simulation of particle dispersion in the wake of a circular cylinder. Aerosol Sci. Technol. 43 (2), 174–187.

Zhao, M., Cheng, L., 2008. Numerical modeling of local scour below a piggyback pipeline in currents. J. Hydraul. Eng. 134 (10), 1452–1463.